RESPONSES TO REVIEWERS' COMMENTS

General Response to the Reviewers:

We appreciate your comments on the manuscript entitled "Using different assumptions of aerosol mixing state and chemical composition to predict CCN concentrations based on field measurements in urban Beijing". All comments were valuable and helped us improve our manuscript. Below are point-by-point responses to the reviewers' comments.

This is an interesting and important study, where a closure between directly measured and calculated CCN concentrations is presented. Overall, the authors did a good job addressing the issues from the previous submission. However, several minor issues have remained. I suggest a minor revision before the paper can be accepted.

In the abstract, some of the abbreviations are left undefined. For instance, it takes some effort to realize that 'EI-SR' stands for 'external-internal size-resolved', as none of those words appear in the abstract.

Re: thanks a lot for the comments. 'EI-SR' is defined as “an assumption of a size dependent chemical composition for which sulfate, nitrate, secondary organic aerosols and aged black carbon are internally mixed with each other but externally mixed with primary organic aerosol and fresh black carbon (EI-SR scheme)”. We have revised this in the abstract.

In CCN equations, a spherical particle geometry is used and hence no assumptions about the type of particle diameter needs to be made. However, the instrument, in general, produce different diameters: mobility diameter from SMPS, volume (or mass) equivalent diameter from SP2, and aerodynamic diameter from AMS. For spherical particles, this makes no difference, but not all particles are spheres. For instance, significant fractions of fresh and aged BC are present in Beijing air. Fresh BC particles are not spheres and neither are some of the partially aged BC. This issue must be addressed.

Re: As the reviewer commented, the instruments produce different diameters. In this paper, we have unified both the aerodynamic diameter from AMS and volume equivalent diameter from SP2 to be mobility diameter. In addition, actual fresh BC particles are not spheres and neither are some of the partially aged BC, but because both the diameter measured from SP2 and the BC size distribution from the literatures are with assumption of the particles being spheres, the fresh and aged BC in this study are thereby assumed to be spherical particles. This issue has been addressed in the revised manuscript (lines 165-175) .

The discussion in lines 159-162 is cryptic and so is the related discussion in lines 435-444. I understand how SP2 underestimates the aged BC particle diameter, but how would it overestimate the diameter? Also, what diameter are we talking about here?

Re: thanks a lot for the comments. Because the SP2 measures BC core diameter instead of the diameter of the BC-containing particle, it would overestimate the BC mass concentration of smaller particles. Such overestimation would likely lead to an underestimation of N_{CCN} due to the increased mass fraction of BC of total particles. Note that, here, it is the "BC mass concentration" rather than "diameter" being overestimated.

Affiliations must be corrected (letters point to wrong institutions)

Re: Revised.

Other minor corrections

L327: remove 'While'

Re: Revised.

L334: replace 'activation' with 'activated'

Re: Revised.

L339: add 'respectively' before 'S*'

Re: Revised.

L386: replace 'most' with 'at least some'

Re: Revised.

L406: replace ‘slight’ with ‘slightly’

Re: Revised.

L408: replace ‘is’ with ‘are’

Re: Revised.

L465: replace ‘internal-’ with ‘internally-’

Re: Revised.

Using different assumptions of aerosol mixing state and chemical composition to predict CCN concentrations based on field measurements in urban Beijing

Jingye Ren[1], Fang Zhang[1, 2*], Yuying Wang[1], Don Collins[3], Xinxin Fan[1], Xiaoai Jin[1], Weiqi Xu[3, 4], Yele Sun[3, 4], Maureen Cribb[5], Zhanqing Li[1, 5]

[1]~~*State Key Laboratory of Earth Surface Processes and Resource Ecology,*~~ *College of Global Change and Earth System Science, Beijing Normal University, Beijing 100875, China*

[2]*Joint Center for Global Change Studies (JCGCS), Beijing 100875, China*

[3]*Department of Atmospheric Sciences, Texas A&M University, College Station, TX, USA*

[4]*State Key Laboratory of Atmospheric Boundary Layer Physics and Atmospheric Chemistry, Institute of Atmospheric Physics, Chinese Academy of Sciences, Beijing 100029, China*

[5]*University of Chinese Academy of Sciences, Beijing 100049, China*

[6]*Earth System Science Interdisciplinary Center and Department of Atmospheric and Oceanic Science, University of Maryland, College Park, Maryland, USA*

Correspondence to: **Fang Zhang (fang.zhang@bnu.edu.cn)**

Abstract

Understanding the impacts of aerosol chemical composition and mixing state on cloud condensation nuclei (CCN) activity in polluted areas is crucial for accurately predicting the CCN number concentrations (N_{CCN}). In this study, we predict N_{CCN} under five assumed schemes of aerosol chemical composition and mixing state based on field measurements in Beijing during the winter of 2016. Our results show that the best closure is achieved with an assumption of a size dependent chemical composition for which sulfate, nitrate, secondary organic aerosols and aged black carbon ~~(BC)~~ are internally mixed with each other but externally mixed with primary organic aerosol ~~(POA)~~ and fresh black carbon~~BC~~ (external-internal size-resolved, abbreviated as EI-SR scheme). The resulting ratios of predicted-to-measured N_{CCN} ($R_{CCN\_p/m}$) were 0.90–0.98 under both clean and polluted conditions. Assumption of an internal mixture and bulk chemical composition (INT-BK scheme) shows good closure with $R_{CCN\_p/m}$ of 1.01–1.16 under clean conditions, implying that it is adequate for CCN prediction in continental clean regions. On polluted days, assuming the aerosol is internally mixed and has a chemical composition that is size dependent (INT-SR scheme) achieves better closure than the INT-BK scheme due to the heterogeneity and variations in particle composition at different sizes. The improved closure achieved using the EI-SR and INT-SR assumptions highlight the importance of measuring size-resolved chemical composition for CCN predictions in polluted regions. N_{CCN} is

significantly underestimated (with $R_{CCN\_p/m}$ of 0.66–0.75) when using the schemes of external mixtures with bulk (EXT-BK scheme) or size-resolved composition (EXT-SR scheme), implying that primary particles experience rapid aging and physical mixing processes in urban Beijing. However, our results show that the aerosol mixing state plays a minor role in CCN prediction when the κ_{org} exceeds 0.1.

1 Introduction

Atmospheric aerosol particles can serve as cloud condensation nuclei (CCN) and, in turn, affect the optical and microphysical properties of clouds (Twomey, 1977; Albrecht, 1989; Charlson et al., 1992). Additionally, an increase in the aerosol number concentration may suppress precipitation in shallow clouds and promote it in deep convective clouds (Rosenfeld et al., 2008; Li et al., 2011). A key challenge to understanding indirect aerosol effects is quantifying CCN spectra and their spatial and temporal variations.

The ability of particles to act as CCN mainly depends on their size, chemical composition, and mixing state (McFiggans et al., 2006; Dusek et al., 2006; Ma et al., 2013). The impacts of the size distribution and chemical composition on CCN activity has been discussed in previous studies (Dusek et al., 2006, Ervens et al., 2007; Broekhuizen et al., 2006; Yum et al., 2005, 2007; Wiedensohler et al., 2009; Deng et al., 2013; Zhang et al., 2014, 2016; Kawana et al., 2016). The effect of chemical composition can be represented by a hygroscopicity parameter (κ) (Petters and Kreidenweis, 2007) that is often used to predict N_{CCN} (Moore et al., 2012; Zhang et al.,

147 2014). However, particle composition may vary from single species to a mixture of
148 multiple species for a given size. A description of size-resolved chemical composition
149 thus leads to a better prediction of N_{CCN} because it allows variation of κ with size
150 (Medina et al., 2007; Wang et al., 2010; Meng et al., 2014). Variations in mixing state
151 also impact N_{CCN} prediction, with the effect dependent on the hygroscopicity of the
152 organic component (Wang et al., 2010). The assumption of internal mixtures has been
153 demonstrated to predict N_{CCN} well (Ervens et al., 2007; Chang et al., 2007; Andreae
154 and Rosenfeld, 2008; Gunthe et al., 2009; Rose et al., 2008; Meng et al., 2014; Zhang
155 et al., 2014; Li et al., 2017). However, some studies have shown that detailed
156 information about the chemical composition and the mixing state is required because
157 of the complexity of the hygroscopicity of organics (Broekhuizen et al., 2006; Bhattu
158 and Tripathi, 2015) and the differences in the CCN activity between fresh and aged
159 aerosols (Gunthe et al., 2011). Therefore, the impact of different assumptions
160 concerning the mixing state and chemical composition on accurately quantifying CCN
161 concentrations needs further investigation, especially in heavily polluted regions.

162 Beijing, a typical polluted city, frequently experiences severe haze pollution
163 episodes (Sun et al., 2013; Guo et al., 2014; Zheng et al., 2015), particularly in winter.
164 Several recent studies have focused on studying particle hygroscopicity (Wu et al.,
165 2016; Wang et al., 2017) and chemical composition (Gunthe et al., 2011), and using
166 bulk κ to predict CCN in Beijing (e.g., Liu et al., 2014; Zhang et al., 2017). However,
167 to our knowledge, a comprehensive CCN closure test considering chemical
168 composition and mixing state is lacking for this polluted urban area. In particular, the

169 transformation of the particle mixing state may be very quick during severe pollution
170 conditions (Wu et al., 2016). During pollution events, the hygroscopicity of organics
171 and the CCN activity are often enhanced rapidly with the aging process (Gunthe et al.,
172 2011; Kawana et al., 2016). Therefore, the characterization and parameterization of
173 CCN activation may be more challenging in polluted regions due to the impacts of
174 organics (Wang et al., 2010; Meng et al., 2014; Che et al., 2016; Zhang et al., 2016).

175 In this study, we use size-resolved measurements of CCN activity and
176 size-resolved chemical composition information to predict N_{CCN} using field
177 measurement data collected in Beijing during the winter of 2016. The CCN closure
178 study is carried out using five schemes with different assumptions of particle mixing
179 state and chemical composition. By classifying the data into three different periods
180 (nighttime, noontime, and the evening rush hour), we also investigate the variations in
181 aerosol mixing state from fresh to relatively aged aerosols. The sensitivity of
182 predicted N_{CCN} to the particle mixing state and organic volume fraction with the aging
183 of organic particles is also presented in the last section of the study.

184 **2 Measurements and data**

185 Data used here were measured from 15 November to 14 December 2016
186 during the Air Pollution and Human Health (APHH) field campaign at the Institute of
187 Atmospheric Physics (IAP), Chinese Academy of Sciences (39.97°N, 116.37°E),
188 which is a typical urban site with influences from traffic and cooking emissions (Sun
189 et al., 2015). The sampling instruments were placed in a container at ground level.

The particle number size distribution (PNSD) was measured by a Scanning Mobility Particle Sizer (SMPS; Wang et al., 2003). The SMPS consists of a differential mobility analyzer (DMA; model 3081, TSI Inc.) and a condensation particle counter (CPC; model 3772, TSI Inc.). Measurements of size-resolved CCN efficiency spectra were made by an integrated system combining the SMPS (Wang et al., 2003) and a Droplet Measurement Technologies CCN counter (DMT-CCNc; Lance et al., 2006). The procedure to couple the SMPS and the DMT-CCNc developed by Moore et al. (2010) was followed. Atmospheric particles were sampled from an inlet located 1.5 m above the roof of the container and were then passed through a silica gel desiccant drying tube and into the SMPS. The relative humidity of the sample flow was below 30%. The sample flow exiting the DMA was divided into 0.5 lpm for the CCNc and 0.5 lpm for the CPC. Before and after the field campaign ammonium sulfate was used to calibrate the supersaturation (SS) levels of the CCNc with longitudinal temperature differences of 2, 3, 5, 8, 10, 13, and 15 K as shown in Fig. S1. Based on this calibration, the five effective SS levels were 0.12, 0.14, 0.23, 0.40, and 0.76%.

The PNSD spanned the size range of 10–550 nm with a measurement scan time of 5 min. Total particle or condensation nuclei (CN) size distributions were calculated with the multiple charge correction and transfer function used in the TSI-AIM software. The CN number concentration (N_{CN}) is the total aerosol number concentration and is obtained by integrating the PNSD over the size range of 10–550 nm. The full measurement cycle of the CCNc for the five SS levels took one hour (20

212 min for 0.12% and 10 min for each higher SS). Size-resolved CCN efficiency data
213 were inverted with a multiple charge correction (Moore et al., 2010). The CCN
214 number size distribution was calculated by multiplying the CCN efficiency spectrum
215 by the particle number size distribution. The total CCN concentration was then
216 calculated by integrating the size-resolved N_{CCN}. The bulk activation ratio (AR) was
217 calculated as N_{CCN}/N_{CN}. The results were stratified between polluted and background
218 conditions with an assumed threshold PM1 mass concentration of 50 μg m^{-3}.

219 An Aerodyne High-Resolution Time-of-Flight Aerosol Mass Spectrometer
220 (HR-ToF-AMS; DeCarlo et al., 2006) was housed in a sampling room on the rooftop
221 of a two-story building to measure size-resolved non-refractory submicron aerosols,
222 including organics, sulfate, nitrate, ammonium, and chloride with a time resolution of
223 ~5 min. More details about the HR-ToF-AMS and the measurement site have been
224 described in previous studies (Sun et al., 2010; Sun et al., 2016). The organics are
225 classified by using Positive Matrix Factorization (PMF) （Paatero and Tapper,1994）,
226 considering as being composed of two components: primary organic aerosol (POA)
227 representing non-hygroscopic particles ~~($\kappa = 0$)~~ and secondary organic aerosol (SOA)
228 representing hygroscopic particles. The first component~~factor~~ consists manily of ~~is~~
229 hydrocarbon-like organic aerosol (HOA) ~~which is considered,~~ a surrogate of primary
230 organic aerosol~~OA~~ (POA) from local~~urban~~ combustion sources. And t~~T~~he size
231 distribution of the primary OA~~HOA~~ was ~~calculated~~ measured ~~from~~ by the estimated
232 size-distribution of the $C_4H_9^+$ fragment ~~which is generally dominated by HOA~~ (Aiken
233 et al., 2009; Zhang et al., 2005). The size distribution of the SOA was calculated~~is~~

~~estimated~~ as the difference between the ~~those of~~ total OA and PH~~H~~OA.

The black carbon (BC) mass concentration was measured using a seven-wavelength aethalometer (AE33, Magee Scientific Corp.). Zhao et al. (2017) provides details about this instrument and the measurements it makes. Due to an absence of size-resolved BC measurements, the BC size distribution was calculated from the combination of an approximately lognormal distribution measured by a single particle soot photometer (SP2, DMT) (Wu et al., 2017) and the total BC mass concentration. Note that because the SP2 measures BC core diameter instead of the diameter of the BC-containing particle, it would overestimate the BC mass concentration of smaller particles but underestimate that of the larger ones. Such overestimation would likely lead to an underestimation of N_{CCN} due to the increased mass fraction of BC of total particles. –The uncertainty of this effect is evaluated in Section 4.3. The fresh and aged BC size distributions are determined from the total BC size distribution measured by the SP2 (Wu et al., 2017) and from the dependence of the fraction of internally mixed soot (F_{in}) on particle diameter (D_p) observed in urban Beijing by Cheng et al. (2012). The instruments produce different diameters. In this paper, we have unified both the aerodynamic diameter from AMS and volume equivalent diameter from SP2 to be mobility diameter. In addition, actual fresh BC particles are not spheres and neither are some of the partially aged BC, but because both the diameter measured from SP2 and the BC size distribution from the literatures are with assumption of the particles being spheres, the fresh and aged BC in this study are thereby assumed to be spherical particles. ~~And the fresh and aged BC are all~~

~~assumed to be spherical particles. Due to the different diameters producing by the instrument, the aerodynamic diameter from AMS and volume equivalent diameter from SP2 are adjusted to be mobility diameter.~~

3 Theory

3.1 Calculation of CCN concentration using *κ*-Köhler theory

In this study, we used the critical or cutoff particle diameter (D_{cut}) and particle number size distribution to calculate N_{CCN}. The method to derive D_{cut} is based on *κ*-Köhler theory (Petters and Kreidenweis, 2007), with the water vapor saturation ratio over the aqueous solution droplet S given by:

$$S = \frac{D^3 - D_P^3}{D^3 - D_P^3(1-\kappa)} \exp\left(\frac{4\sigma_w M_w}{RT\rho_W D}\right), \quad (1)$$

where D is the droplet diameter, D_p is the dry diameter of the particle, M_w is the molecular weight of water, σ_w is the surface tension of pure water, ρ_w is the density of water, R is the gas constant, and T is the absolute temperature. When $\kappa > 0.1$ it can be approximately expressed as:

$$\kappa = \frac{4A^3}{27 D_p^3 \ln^2 S_c}, \quad (2)$$

$$A = \frac{4\sigma_w M_w}{RT\rho_w}, \quad (3)$$

where S_c is the particle critical supersaturation. The other variables in the equations

are: T = 298.15 K, R = 8.315 J K^{-1} mol^{-1}, ρ_w = 997.1 kg m^{-3}, M_w = 0.018015 kg mol^{-1}, and σ_w = 0.072 J m^{-2} (Rose et al., 2008).

For internally-mixed particles, κ is calculated as follows (Petters and Kreidenweis, 2007; Gunthe et al., 2009):

$$\kappa_{chem} = \sum_i \varepsilon_i \kappa_i , \quad (4)$$

$$\kappa_{org} = f_{POA} \cdot \kappa_{POA} + f_{SOA} \cdot \kappa_{SOA} , \quad (5)$$

where κ_i and ε_i are the hygroscopicity parameter and volume fraction for the individual components in the mixture, and f_{POA} and f_{SOA} are the primary organic aerosol (POA) and secondary organic aerosol (SOA) mass fractions in the mixture. The Aerosol Mass Spectrometer (AMS) mainly measured the particle mass size distributions of SO_4^{2-}, NO_3^-, NH_4^+ and organic compounds, while the Zdanovskii-Stokes-Robinson relation requires the volume fractions of the particle chemical composition (Stokes and Robinson, 1966; Zdanovskii, 1948). A simplified ion pairing scheme is used to calculate the mass concentrations of the inorganic salts, which includes only NH_4NO_3 and $(NH_4)_2SO_4$ as possible salts (Gysel et al., 2007). In this study, we considered five components: NH_4NO_3, $(NH_4)_2SO_4$, SOA, POA, and BC. The $\kappa_{(NH4NO3)}$ is equal to 0.67 and $\kappa_{((NH4)2SO4)}$ is equal to 0.61 (Petters and Kreidenweis, 2007; Gunthe et al., 2009). The κ_{org} is estimated using the linear function derived by Mei et al. (2013a), namely, $\kappa_{org} = 2.10 f_{44} - 0.11$, where f_{44} is dependent upon organics oxidation level. The mean κ_{org} is 0.10 in our case. The organics are classified into ~~by~~

~~using Positive Matrix Factorization (PMF; Paatero and Tapper,1994) , and considered to be composed of~~ two factors~~components~~: POA representing non-hygroscopic particles (κ = 0) and SOA representing hygroscopic species. In our study, the average contributions of POA and SOA to total organics were 0.53 and 0.47, respectively. On the basis of equation (5), $\kappa_{(SOA)}$ is assumed to be 0.2. Also, $\kappa_{(BC)}$ is assumed to be 0.

3.2 Assumptions about mixing state and chemical composition

To examine the influence of the mixing state and chemical composition on CCN activation, five assumptions (Fig. 1) are used to predict N_{CCN}. Although the assumption of completely internal or external mixing for ambient aerosols represents two extremely simplified schemes and may be atmospherically unrealistic, it allows us to understand the importance of the particle mixing state for predicting N_{CCN}. In addition, size independent and dependent compositions are derived from the mass concentrations of different species measured by the AMS so that the impact of chemical composition on CCN activity can be examined. A detailed introduction of the five assumption schemes follows.

Assumption 1: internal mixture with bulk chemical composition (INT-BK)

In this scheme, submicron particles are assumed to be internally mixed with bulk chemical composition, where the mass fraction of each component (e.g. NH_4NO_3, $(NH_4)_2SO_4$, SOA, POA, and BC) is uniform throughout the full size range as shown in Fig. 1a. The overall κ is calculated from the bulk chemical composition measured by

the AMS based on the simple mixing rule (Equation 4) to obtain the critical diameter at a given SS. For calculating N_{CCN} all (and only) particles with diameters greater than D_{cut} are considered CCN-active. The total N_{CCN} is then calculated from the step-wise integration of the PNSD for $D_p > D_{cut}$. The equations used in the calculations are as follows,

$$CCN_{pre} = \int_{D_{cut}}^{D_{end}} n(\log D_p) d \log D_p \quad (6)$$

$$D_{cut} = \sqrt[3]{\frac{4A^3}{27 \sum_i \varepsilon_i \kappa_i \ln^2 S_c}} \quad (7)$$

where D_{cut} is the critical diameter, D_{end} is the upper size limit of the PNSD, n (log D_p) is the function of the aerosol number size distribution, i is the chemical component element, and the other parameters are the same as those presented in Equations (2), (3) and (4).

Assumption 2: internal mixture with size-resolved chemical composition (INT-SR)

For this scheme submicron particles are assumed to be internally mixed and the chemical composition is size-dependent as shown in Fig. 1d. The fractional contributions of the components at each size bin are derived from mass size distributions of the five species considered, i.e., NH_4NO_3, $(NH_4)_2SO_4$, SOA, POA, and BC.

For this assumption, the critical diameter is derived from the total hygroscopic parameter, κ, at each size bin, j. For each size bin for which $D_{p,j}$ is > than the calculated $D_{cut,j}$ the activated fraction was assumed to be 1.0 and for all others it was 0.0. The N_{CCN} is calculated as follows:

$$CCN_{pre} = \int_{D_{begin}}^{D_{end}} n(\log D_p) d \log D_p \quad (8)$$

$$D_{cut,j} = \sqrt[3]{\frac{4A^3}{27 \sum_i \varepsilon_{ij} \kappa_{ij} \ln^2 S_c}} \quad (9)$$

where D_{begin} and D_{end} are the first and last diameters of the PNSD, n ($\log D_p$) is the function of the aerosol number size distribution, i is the chemical component element, j is the PNSD size bin, and the other parameters are the same as those presented in Equations (2), (3) and (4).

Assumption 3: external mixture with bulk chemical composition (EXT-BK)

For this scheme the submicron aerosol is treated as an external mixture. This means that there are five types of particles, i.e., NH_4NO_3, $(NH_4)_2SO_4$, SOA, POA, and BC, and each particle consists of a single component. The volume fraction of each component, which is derived from bulk mass concentrations, does not vary with size (as shown in Fig. 1b).

At a given S, the critical diameter of each particle type is retrieved from the κ of each component. The N_{CCN} of each aerosol type is calculated as the CCN-active

particle number concentration multiplied by the bulk volume fraction of the components as expressed in Equation (10). The N_{CCN} of the five particle types are finally summed to obtain the total N_{CCN}. The specific equations are as follows,

$$CCN_{pre} = \sum_{i} \left(\int_{D_{icut}}^{D_{end}} n(\log D_p) d \log D_p * V_i \right) \quad (10)$$

$$D_{cut,i} = \sqrt[3]{\frac{4A^3}{27\kappa_i \ln^2 S_c}} \quad (11)$$

where $D_{cut,i}$ is calculated for each component, i, at a given SS, V_i is the volume fraction of each aerosol type, n ($\log D_p$) is the function of the aerosol number size distribution, i is the chemical component element, and the other parameters are the same as those presented in Equations (2), (3) and (4).

Assumption 4: external mixture with size-resolved chemical composition (EXT-SR)

As with the EXT-BK scheme the same five particle types are considered and their relative concentrations selected to match the measured composition. But unlike with the EXT-BK scheme the relative concentrations of the five particle types vary with particle size to capture the size-dependence of the measured composition, as is depicted in Fig. 1e. The volume fraction of each particle type at each size is first multiplied by the total particle number size distribution (PNSD) to get the $PNSD_i$ of each aerosol type. The N_{CCN} of each particle type is then obtained from the step-wise

integration of the $PNSD_i$ for $D_p > D_{cut,i}$, and then summed to get the total $N_{CCN,}$ as described by Equation (12). Similar to EXT-BK, the critical diameter of each particle type is also derived from the κ of each pure component at a given S.

$$CCN_{pre} = \sum_{i} \left(\int_{D_{begin}}^{D_{end}} (n(\log D_p) * V_{ij}) d \log D_p \right) \quad (12)$$

$$D_{cut,i} = \sqrt[3]{\frac{4A^3}{27\kappa_i \ln^2 S_c}} \quad (13)$$

where V_i is the volume fraction of each particle type in a size bin, n ($\log D_p$) is the function of the aerosol number size distribution, *i* is the chemical component element, *j* is the particle size bin, and the other parameters are the same as those presented in Equations (2), (3) and (4).

Assumption 5: sulfate, nitrate, SOA and aged BC internally mixed, and POA and fresh BC externally mixed, and all components with size-resolved chemical composition (EI-SR)

At each particle size sulfate, nitrate, and SOA with BC-aged are treated as internally mixed, but POA and BC-fresh are present in separate particles and are non-hygroscopic. As with INT-SR and EXT-SR the chemical composition is size-dependent, as shown in Fig. 1c. The EI-SR scheme likely represents a case that is most similar to that of actual atmospheric aerosols in locations such as Beijing. The fresh and aged BC size distributions are determined from the total BC size

distribution measured by the SP2 (Wu et al., 2017) and from the dependence of the fraction of internally mixed soot (F_{in}) on particle diameter (D_p) observed in urban Beijing by Cheng et al. (2012).

In this assumption the fresh BC and POA particles can serve as CCN only if their diameter is larger than 200 nm; otherwise they are CCN-inactive. Thus, the total N_{CCN} of those externally mixed components (N_{CCN}_EXT) is calculated from the step-wise integration of the product of the PNSD and the volume fraction of the fresh BC and POA in each size bin larger than 200 nm.

The N_{CCN} of the remaining components (sulfate, nitrate, and SOA with BC-aged) that are treated as an internal mixture, denoted as N_{CCN}_INT, is predicted in the same way as for the INT-SR scheme, with the only difference being that the PNSD is first multiplied by the volume fraction of the mixed component particles for each size bin. The total N_{CCN} is thus calculated as the sum of N_{CCN}_EXT and N_{CCN}_INT. The specific equations are as follows,

$$CCN_{pre} = \int_{D_{begin}}^{D_{200}} (n(\log D_p) * r_j) d \log D_p + \int_{D_{200}}^{D_{end}} n(\log D_p) d \log D_p \quad (14)$$

$$D_{cut,j} = \sqrt[3]{\frac{4A^3}{27 \sum_i \varepsilon_{ij} \kappa_{ij} \ln^2 S_c}} \quad (15)$$

where D_{begin} and D_{end} are the first and last diameters of the PNSD, n ($\log D_p$) is the function of the aerosol number size distribution, r is the volume fraction of the internal (hygroscopic) mixture at each size, i is the chemical component element, j is

the particle size bin, and the other parameters are the same as those presented in Equations (2), (3) and (4).

4 Results and discussion

4.1 Diurnal variations in aerosol properties

Diurnal variations in mean PNSD and bulk chemical composition under polluted and background conditions are shown in Fig. 2. Significant diurnal variations in PNSD are observed during the campaign. For both polluted and background cases the abrupt increases in concentration of small particles (D_p < 100 nm) from 1700–2000 local time (LT) are likely related to fresh primary emissions from cooking and traffic sources (Wang et al., 2017; Zhao et al., 2017), which is also evident in the significant increase in mass concentration of non-hygroscopic POA (Fig. 2d and 2e). The peak amplitude in the PNSD that occurs from about 0800 to1200 LT is probably associated with secondary formation processes, which is indicated by an apparent increase of nitrate, SOA and f_{44} (oxidation level of organics) in the morning (0800 LT) when photochemistry becomes significant. The effect is more apparent on clean days. In addition, the PNSD amplitude and BC and POA concentrations are high at nighttime, suggesting an influence from the diurnal variation of the planetary boundary layer (PBL) height. In particular, on polluted days the PBL plays a key role in regulating the diurnal variation of primary components like POA and BC (e.g., Dzepina et al., 2009; Cross et al., 2009). ~~While o~~On clean days secondary formation

and primary sources play dominant roles in regulating diurnal variations. The PNSD in clean cases has peaks at smaller D_p (~30–40 nm, Fig. 1c) compared to polluted cases (~100 nm), which is associated with particle growth accompanying atmospheric chemistry processes during haze evolution (Guo et al., 2014; Wang et al., 2016).

4.2 Cumulative Gaussian distribution function fit and parameters derived from the CCN efficiency

The ~~activation~~ activated fractions measured at the five supersaturation levels were fitted using the following two functions (Rose et al., 2008; Mei et al., 2013b):

$$R_a(S) = \frac{E}{2} \cdot (1 + erf(\frac{\ln S - \ln S^*}{\sqrt{2\sigma_S^{\,2}}})), \quad (16)$$

$$f_{N_{CCN}/N_{CN}} = a(1 + erf(\frac{D - D_a}{\sigma_a \sqrt{2}})), \quad (17)$$

where $Ra(S)$ and $f(_{NCCN/NCN})$ are the CCN activation fractions, the maximum activation fraction (MAF) is equal to E or $2a$, S^* and D_a are the midpoint activation supersaturation and diameter, respectively, and σ_s and σ_a are the cumulative distribution function (CDF) standard deviations. During this field campaign, 2580 size-resolved CCN efficiency spectra at five SS levels were measured. To illustrate the characteristics of the activation spectra, the CDF fits are shown in Fig. 3 and in Tables S1-2. A gradual increase in size-resolved AR with SS suggests that particles had different hygroscopicities even at the same diameter. The heterogeneity of particle

chemical composition can be represented by the ratio of σ_a and D_a (i.e., σ_a/D_a), where σ_a is the standard deviation derived from the cumulative Gaussian distribution function (Eqn. 12) and D_a is the activation diameter (Rose et al., 2010). The ratio of σ_a/D_a during the three periods is shown in Fig. 3b.

4.2.1 CCN activation curves and heterogeneity of chemical components

For larger particles with $D_p > 100$ nm, no significant differences were observed in the CCN efficiency spectra (Fig. 3a), suggesting a similar hygroscopicity during the three periods. For particles with $D_p < 100$ nm, the CCN efficiency spectrum observed during the evening rush hour period showed a much more gradual increase (with smaller slopes) in size-resolved AR than that derived for the other two periods. This is attributed to the strong influence of POA emissions, which consist of less hygroscopic and externally-mixed smaller particles mainly from cooking and traffic during the evening rush hour period (also indicated by the increased σ_a/D_a). Particles with $D_p <$ 100 nm emitted during the evening rush hour period require a higher SS to reach the same AR. However, for $D_p > 100$ nm the slope of AR with respect to SS was steep and near the instrumental limit obtained for a pure ammonium sulfate aerosol. Che et al. (2016) have reported that particles larger than about 150 nm have relatively uniform composition. This suggests that particles become more internally mixed with growth from the Aitken mode to the accumulation mode. This feature is also suggested by the decreasing σ_a/D_a with increasing particle diameter.

4.2.2 Mean critical activation diameter

The critical activation diameter at different SS levels under background and polluted conditions is shown in Fig. 4. The difference in critical diameter between polluted and background cases are calculated as D_p_POL - D_p_BG. At lower SS levels, the critical diameters for polluted cases were slightly smaller than those observed on clean days, suggesting larger particles are more CCN-active on polluted days. This is expected based on HTDMA measurements that showed that particles in the accumulation mode on polluted days are more hygroscopic than those on clean days in urban Beijing (Wang et al., 2017). At higher SS the critical diameter on polluted days was a little higher than that obtained under clean conditions, suggesting that particles with D_p of ~40 nm are less CCN active. This is likely because a high concentration of small and hygroscopic particles in the Aitken mode arise from the photochemistry-driven nucleation process on clean days. However, in polluted cases, small particles are mostly composed of hydrophobic POA from cooking and traffic sources. This was also observed by Wang et al., (2017) who showed that 40 nm particles are less hygroscopic on polluted days. However, the differences in critical diameter between polluted and background cases are small, reflecting a relatively minor influence of hygroscopicity on CCN activity.

4.2.3 MAF

As shown in Fig. 5, the maximum activated fractions on clean and polluted days

during the campaign are less than 1, which suggests that at least some~~most~~ sampled aerosols were externally mixed (Gunthe et al., 2011). For example, the MAF for particles with D_p of ~180 nm was around 0.78 at SS = 0.12% under background conditions, indicating that ~22% of the particles are non-hygroscopic. The higher MAFs under polluted conditions suggest a more internally mixed aerosol (Wu et al., 2016; Wang et al., 2017). The MAF during the 1200–1400 LT period was highest, which is likely due to strong photochemical aging processes that lead to more internal mixing of the aerosol.

4.3 CCN closure study and the sensitivity of predicted N_{CCN} to assumed aerosol mixing state and chemical composition

Fig. 6 shows the comparisons between predicted and measured N_{CCN} at different SS levels under background and polluted conditions. The ratios of predicted-to-measured N_{CCN} ($R_{CCN\_p/m}$) ranged from 0.66 to 1.16, suggesting significant influences of the different assumptions on CCN prediction. The EI-SR assumption scheme predicts N_{CCN} very well, with $R_{CCN\_p/m}$ of 0.90–0.98 (corresponding to a slight underestimation of 2-10%). For the EI-SR scheme, hydrophobic POA and a portion of the BC are assumed to be externally mixed while the other species (sulfate, nitrate, SOA and aged BC) are assumed to be internal mixtures. The assumption is physically sound, and the result just implies that the EI-SR represents well the actual mixing state and compositions of the particles. The slight underestimation may due to an overestimation of fresh BC caused by the

503 method (see Section 3.1) that we used to retrieve it. Also, a slightly larger
504 underestimation of N_{CCN} for BG case in EI-SR scheme showed in Figure 6 may
505 suggest that aerosols during clean periods are~~is~~ mostly aged and internal-mixed.

506 The INT-SR and INT-BK schemes that assume the aerosol is internally mixed also
507 predict N_{CCN} reasonably well at lower SS. The prediction is better on background days,
508 reflecting the more homogenous aerosol composition in clean conditions. With
509 increasing SS this overestimation became more pronounced, which is likely due to
510 limitations of the AMS measurements. The AMS distributions show that the mass
511 concentration was most impacted by particles with diameters near ~100–400 nm.
512 Because particles in that size range tended to be more hygroscopic than those with
513 diameters < 100 nm, this leads to an overestimation of κ (underestimation of the
514 critical diameter) and a resulting overestimation of N_{CCN} at high SS. With decreasing
515 SS the critical diameter increased and the deviation using the INT-BK and INT-SR
516 schemes decreased. Detailed explanations about this effect have been given by Wang
517 et al. (2010) and Zhang et al. (2017). Overall, the INT-BK and INT-SR schemes
518 achieve CCN closure within what is deemed here an acceptable overprediction of
519 0-16%. The EXT-BK and EXT-SR schemes underestimated N_{CCN}, with $R_{CCN\_p/m}$ of
520 0.66-0.75.

521 Overall, the internal-mixing schemes achieve much better closure than do those
522 assuming external mixtures. Our results suggest that freshly-emitted particles in
523 urban Beijing may experience a quick conversion and mixing with pre-existing

secondary particles, e.g. converting from externally mixed to internally mixed (or from hydrophobic to hydrophilic, along with a decrease in the volume of POA and BC) as reported previously (Riemer et al., 2004; Aggarwal and Kawamura, 2009; Jimenez et al., 2009; Wu et al., 2016; Peng et al., 2016). In summary, under background conditions, the INT-BK scheme achieved the best CCN closure, implying that the INT-BK assumption is likely sufficient to predict CCN in clean continental regions. However, in polluted regions, the EI-SR and INT-SR schemes may achieve better closure.

As mentioned in Section 2.2, because the SP2 measures BC core diameter and not the diameter of the BC-containing particle, the method would overestimate the BC mass concentration of smaller particles but underestimate that of the larger ones. This effect adds uncertainty to the CCN prediction when using the EXT-SR scheme and is evaluated here (Fig. 7). For the evaluation, we predict N_{CCN} with the retrieved fresh BC size distribution only in the EXT-SR scheme, which represents an upper limit of the overestimation of the fresh BC size distribution due to the SP2 measurement. Therefore, the result represents the largest underestimation of N_{CCN} caused by the BC-containing particle effect. Our result shows that the underestimation of N_{CCN} is reduced from 28% to 25% by changing the total BC size distribution to that of just the fresh BC. That means that the overestimation of fresh BC due to the BC-containing particle effect in the SP2 measurements would lead to a maximum underestimation of 3% of N_{CCN}. The minimal uncertainty contributed by uncertainty in the BC size distribution could be explained by the small fractional contribution of BC to the total

546 particle concentration. In conclusion, such an effect is quite small or negligible
547 compared to the overall large underestimation of N_{CCN} with the EXT-SR assumption.

548 **4.4 Performance of the five schemes at different times of the day**

549 To investigate the performance of the five schemes at different times of the day,
550 the diurnal variations in the $R_{CCN\_p/m}$ (SS = 0.23%) derived by the schemes are shown
551 in Fig. 8. In general, the INT-BK, INT-SR, and EI-SR schemes can predict N_{CCN}
552 well during all periods of the day under polluted or background conditions. $R_{CCN\_p/m}$
553 values are within the acceptable ±20% uncertainty range (Wang et al., 2010; Zhang
554 et al., 2017). Compared with other periods, the predicted N_{CCN} during the morning
555 and evening rush hour periods showed the most sensitivity to the different assumption
556 schemes, especially on clean days (Fig. 8b). For example, the $R_{CCN\_p/m}$ derived using
557 the INT-SR schemes reaches values up to >1.2, and the $R_{CCN\_p/m}$ obtained using the
558 EXT-BK scheme decreased to a minimum value of ~0.5. The INT-SR, INT-BK and
559 EI-SR assumptions overestimate N_{CCN} for the evening rush hour period by up to
560 ~20%. This may be because most freshly emitted POA and BC particles during
561 evening traffic hours are hydrophobic and do not contribute to the N_{CCN}. In addition,
562 for EIS assumption, a portion of BC is assumed aged and internally-mixed with
563 sulfate, nitrate and SOA, as may reduce the actual fraction of fresh BC during rush
564 hour period and thereby lead to an overestimation of N_{CCN}.

565 Use of the EXT-BK or EXT-SR assumption for the polluted case resulted in a
566 predicted N_{CCN} that was underestimated by ~30-40% at night (0000–0600 LT).

Expectedly, the prediction using the two schemes improved during the daytime and evening rush hours, e.g., the $R_{CCN\_p/m}$ changed from about 0.6 to 0.8. This is likely associated with heavy urban traffic emissions/residential cooking sources during the daytime that lead to more externally-mixed particles under polluted conditions; while, at night, the particles are less influenced by those local primary sources (Zhao. et al., 2017). Wang et al. (2017) showed that the probability density function of κ during rush hour has a bimodal distribution and a hydrophobic mode from locally-emitted particles. This also leads to reasonably accurate estimates of N_{CCN} during nighttime with larger error during the daytime when using the internal mixing assumptions (INT-BK, INT-SR and EI-SR) for polluted cases (Fig. 8).

4.5 Impact of mixing state and organic volume fraction on predicted N_{CCN} and their variation with aerosol aging

To further examine the sensitivity of predicted N_{CCN} to the particle mixing state and organic volume fraction with the aging of organic particles, the relative deviation between N_{CCN} predicted assuming internal and external mixtures as a function of κ_{org} was calculated, with the results shown in Fig. 9. The schemes that assume internal and external mixtures use bulk composition of organics, sulfate, and nitrate, which simplifies the analysis and interpretation of the results. For the data collected throughout the field campaign, the organic volume fraction is categorized as <50%, 50-60%, and >60%. The deviation between the concentrations predicted assuming internal and external mixtures is calculated as [(N_{CCN}.INT-BK - N_{CCN}.EXT-BK)

588 (N_{CCN}.EXT-BK)$^{-1}$]. The result shows that the relative deviation increased as the
589 organic volume fraction increased. For organic volume fractions less than 50% the
590 maximum difference can only reach up to 20% (SS=0.76%). This is consistent with
591 previous studies that reported differences less than 20% when x_{org} < 30%
592 (Sotiropoulou et al., 2006; Wang et al., 2010). The maximum deviation approaches to
593 100% for x_{org} of >60% at SS = 0.76%. Overall, the deviation is largest when the
594 organics are less or non-hygroscopic, i.e., when κ_{org} < 0.05. The deviation decreased
595 rapidly as κ_{org} increased to 0.05 in all cases. For κ_{org} of 0.1 the differences were less
596 than 20%, even with high organic fractions. Moreover, differences were 10% or less
597 for κ_{org} of 0.15, suggesting that the mixing state plays a minor role when κ_{org} exceeds
598 0.1.

599 **5 Conclusions**

600 In this study, we have investigated the importance of aerosol chemical
601 composition and mixing state on CCN activity based on measurements made during a
602 field campaign carried out in Beijing in the winter of 2016. The N_{CCN} was predicted
603 by applying κ-Köhler theory and using five schemes that assume different mixing
604 state and chemical composition combinations.

605 We show that there is a significant impact of the different assumptions on CCN
606 prediction, with $R_{CCN\_p/m}$ ranging from 0.66 to 1.16. The best estimates of N_{CCN} under
607 both background and polluted conditions were obtained when using the EI-SR scheme,
608 with a resulting $R_{CCN\_p/m}$ of 0.90–0.98. Under background conditions, the INT-BK

609 scheme also provided reasonable estimates, with $R_{CCN\_p/m}$ ranging from 1.00–1.16.
610 This suggests that the INT-BK assumption is likely sufficient to predict CCN in clean
611 continental regions. On polluted days, the EI-SR and INT-SR schemes are believed to
612 achieve better closure than the INT-BK scheme due to the heterogeneity in particle
613 composition across different sizes. The improved closure obtained using the EI-SR
614 and INT-SR assumptions highlights the importance of knowing the size-resolved
615 chemical composition for CCN prediction in polluted regions. The EXT-SR and
616 EXT-BK schemes markedly underestimate N_{CCN} on both polluted and clean days,
617 with an $R_{CCN\_p/m}$ of 0.66–0.75. The diurnal variations in $R_{CCN\_p/m}$ show that the
618 predicted N_{CCN} during the evening rush hour period is most sensitive to the mixing
619 state assumptions. The $R_{CCN\_p/m}$ ranged from ~0.5 to ~1.2, reflecting the impact from
620 evening traffic and cooking sources (both with large amounts of hydrophobic POA).
621 But we also find that the particle mixing state plays a minor role when κ_{org} exceeds
622 0.1, even with a high organic fraction.

623 **Acknowledgements.** This work was funded by the NSFC research project (41675141
624 and 91544217), the fundamental Research Funds for the Central Universities, the
625 National Basic Research Program of China '973' (2013CB955800), the NSCF-TAMU
626 Collaborative Research Grant Program (4141101031), and the Natural Science
627 Foundation (NSF) (AGS1534670). We thank all participants of the field campaign for
628 their tireless work and cooperation.

629

References

Aggarwal, S. G., and Kawamura, K.: Carbonaceous and inorganic composition in long-range transported aerosols over northern Japan: Implication for aging of water-soluble organic fraction, Atmos. Environ., 43, 2532–2540, doi:10.1016/j.atmosenv.2009.02.032, 2009.

Albrecht, B. A.: Aerosols, cloud microphysics, and fractional cloudiness, Science, 245, 1227–1230, 1989.

Andreae, M. O., and Rosenfeld, D.: Aerosol–cloud–precipitation interactions. Part 1. The nature and sources of cloud-active aerosols, Earth-Science Reviews, 89, 13–41, doi:10.1016/j.earscirev.2008.03.001, 2008.

Aiken, A. C., Salcedo, D., Cubison, M. J., Huffman, J. A., DeCarlo, P. F., Ulbrich, I. M., Docherty, K. S., Sueper, D., Kimmel, J. R., Worsnop, D. R., Trimborn, A., Northway, M., Stone, E. A., Schauer, J. J., Volkamer, R. M., Fortner, E., de Foy, B., Wang, J., Laskin, A., Shutthanandan, V., Zheng, J., Zhang, R., Gaffney, J., Marley, N. A., Paredes-Miranda, G., Arnott,W. P., Molina, L. T., Sosa, G., and Jimenez, J. L.: Mexico City aerosol analysis during MILAGRO using high resolution aerosol mass spectrometry at the urban supersite (T0) - Part 1: Fine particle composition and organic source apportionment, Atmos. Chem. Phys., 9, 6633– 6653, doi:10.5194/acp-9-6633-2009, 2009.

Bhattu, D., and Tripathi, S. N.: CCN closure study: Effects of aerosol chemical composition and mixing state, J. Geophys. Res. Atmos., 120, 766–783, doi:10.1002/2014jd021978, 2015.

Broekhuizen, K., Chang, R. Y. W., Leaitch, W. R., Li, S. M., and Abbatt, J. P. D.: Closure between measured and modeled cloud condensation nuclei (CCN) using size-resolved aerosol compositions in downtown Toronto, Atmos. Chem. Phys., 6, 2513–2524, 10.5194/acp-6-2513-2006, 2006.

Chang, R. Y. W., Liu, P. S. K., Leaitch, W. R., and Abbatt, J. P. D.: Comparison between measured and predicted CCN concentrations at Egbert, Ontario: Focus on the organic aerosol fraction at a semirural site, Atmos. Environ., 41, 8172–8182, 2007.

Charlson, R. J., Schwartz, S. E., Hales, J. M., Cess, R. D., Coakley, J. A., Jr., Hansen, J. E., and Hofmann, D. J.: Climate forcing by anthropogenic aerosols, Science, 255, 423+, 1992.

Che, H. C., Zhang, X. Y., Wang, Y. Q., Zhang, L., Shen, X. J., Zhang, Y. M., Ma, Q. L., Sun, J. Y., Zhang, Y. W., and Wang, T. T.: Characterization and parameterization of aerosol cloud condensation nuclei activation under different pollution conditions, Sci. Rep, 6, doi:10.1038/srep24497, 2016.

662 Cross, E. S., Onasch, T. B., Canagaratna, M., Jayne, J. T., Kimmel, J., Yu, X. Y., Alexander, M. L.,
663 Worsnop, D. R., and Davidovits, P.: Single particle characterization using a light scattering
664 module coupled to a time of flight aerosol mass spectrometer, Atmos. Chem. Phys., 9,
665 7769–7793, doi:10.5194/acp-9-7769-2009, 2009.

666 Cheng, Y. F., Su, H., Rose, D., Gunthe, S. S., Berghof, M., Wehner, B., Achtert, P., Nowak, A.,
667 Takegawa, N., Kondo, Y., Shiraiwa, M., Gong, Y. G., Shao, M., Hu, M., Zhu, T., Zhang, Y. H.,
668 Carmichael, G. R., Wiedensohler, A., Andreae, M. O., and Pöschl, U.: Size-resolved
669 measurement of the mixing state of soot in the megacity Beijing, China: diurnal cycle, aging
670 and parameterization, Atmospheric Chemistry and Physics, 12, 4477-4491,
671 10.5194/acp-12-4477-2012, 2012.

672 Dall'Osto, M., Harrison, R. M., Coe, H., Williams, P. I., and Allan, J. D.: Real time chemical
673 characterization of local and regional nitrate aerosols, Atmos. Chem. Phys., 9, 3709–3720,
674 10.5194/acp-9-3709-2009, 2009.

675 DeCarlo, P. F., Kimmel, J. R., Trimborn, A., et al.: Field-deployable, high-resolution,
676 time-of-flight aerosol mass spectrometer, Anal. Chem., 78, 8281–8289, 2006.

677 Deng, Z. Z., Zhao, C. S., Ma, N., Ran, L., Zhou, G. Q., Lu, D. R., and Zhou, X. J.: An examination
678 of parameterizations for the CCN number concentration based on in situ measurements of
679 aerosol activation properties in the North China Plain, Atmos. Chem. Phys., 13, 6227–6237,
680 10.5194/acp-13-6227-2013, 2013.

681 Dusek, U., Frank, G. P., Hildebrandt, L., et al.: Size matters more than chemistry for cloud
682 nucleating ability of aerosol particles, Science, 312, 1375–1378, 2006.

683 Dzepina, K., Volkamer, R. M., Madronich, S., Tulet, P., Ulbrich, I. M., Zhang, Q., Cappa, C. D.,
684 Ziemann, P. J., and Jimenez, J. L.: Evaluation of recently proposed secondary organic aerosol
685 models for a case study in Mexico City, Atmos. Chem. Phys., 9, 5681–5709,
686 doi:10.5194/acp-9-5681-2009, 2009.

687 Ervens, B., Cubison, M., Andrews, E., et al.: Prediction of cloud condensation nucleus number
688 concentration using measurements of aerosol size distributions and composition and light
689 scattering enhancement due to humidity, J. Geophys. Res. Atmos., 112, D10S32,
690 doi:10.1029/2006JD007426, 2007.

691 Gunthe, S. S., King, S. M., Rose, D., Chen, Q., Roldin, P., Farmer, D. K., Jimenez, J. L., Artaxo, P.,
692 Andreae, M. O., Martin, S. T., and Pöschl, U.: Cloud condensation nuclei in pristine tropical
693 rainforest air of Amazonia: size resolved measurements and modeling of atmospheric aerosol
694 composition and CCN activity, Atmos. Chem. Phys., 9, 7551–7575,
695 doi:10.5194/acp-9-7551-2009, 2009.

Gunthe, S. S., Rose, D., Su, H., Garland, R. M., Achtert, P., Nowak, A., Wiedensohler, A., Kuwata, M., Takegawa, N., Kondo, Y., Hu, M., Shao, M., Zhu, T., Andreae, M. O., and Pöschl, U.: Cloud condensation nuclei (CCN) from fresh and aged air pollution in the megacity region of Beijing, Atmos. Chem. Phys., 11, 11023–11039, doi:10.5194/acp-11-11023-2011, 2011.

Guo, S., Hu, M., Zamora, M. L., Peng, J., Shang, D., Zheng, J., Du, Z.,Wu, Z., Shao, M., Zeng, L., Molina, M. J., and Zhang, R.: Elucidating severe urban haze formation in China, P. Natl. Acad. Sci. USA, 111, 17373–17378, doi:10.1073/pnas.1419604111, 2014.

Gysel, M., Crosier, J., Topping, D. O., Whitehead, J. D., Bower, K. N., Cubison, M. J., Williams, P. I., Flynn, M. J., McFiggans, G. B., and Coe, H.: Closure study between chemical composition and hygroscopic growth of aerosol particles during TORCH2, Atmos. Chem. Phys., 7, 6131–6144, doi:10.5194/acp-7-6131-2007, 2007.

Jimenez, J. L., Canagaratna, M. R., et al.: Evolution of organic aerosols in the atmosphere, Science, 326, 1525–1529, 2009.

Kawana, K., Nakayama, T., and Mochida, M.: Hygroscopicity and CCN activity of atmospheric aerosol particles and their relation to organics: Characteristics of urban aerosols in Nagoya, Japan, J. Geophys. Res. Atmos., 121, 4100–4121, doi:10.1002/2015jd023213, 2016.

Lance, S., Medina, J., Smith, J., and Nenes, A.: Mapping the operation of the DMT continuous flow CCN counter, Aerosol Sci. Technol., 40, 242–254, 2006.

Li, Y., Zhang, F., Li, Z., Sun, L., Wang, Z., Li, P., Sun, Y., Ren, J., Wang, Y., Cribb, M., and Yuan, C.: Influences of aerosol physiochemical properties and new particle formation on CCN activity from observation at a suburban site of China, Atmos. Res., 188, 80–89, doi:10.1016/j.atmosres.2017.01.009, 2017.

Li, Z., F. Niu, J. Fan, Y. Liu, D. Rosenfeld, and Y. Ding.: The long-term impacts of aerosols on the vertical development of clouds and precipitation, Nature Geosci. 4, doi: 10.1038/NGEO1313, 2011.

Liu, H. J., Zhao, C. S., Nekat, B., Ma, N., Wiedensohler, A., van Pinxteren, D., Spindler, G., Müller, K., and Herrmann, H.: Aerosol hygroscopicity derived from size-segregated chemical composition and its parameterization in the North China Plain, Atmos. Chem. Phys., 14, 2525–2539, doi:10.5194/acp-14-2525-2014, 2014.

Ma, Y., Brooks, S. D., Vidaurre, G., Khalizov, A. F., Wang, L., and Zhang, R..: Rapid modification of cloud-nucleating ability of aerosols by biogenic emissions, Geophys. Res. Lett., 40(23), 6293–6297, 2013.

728 McFiggans, G., Artaxo, P., Baltensperger, U., Coe, H., Facchini, M. C., Feingold, G., Fuzzi, S.,
729 Gysel, M., Laaksonen, A., Lohmann, U., Mentel, T. F., Murphy, D. M., O'Dowd, C. D., Snider,
730 J. R., and Weingartner, E.: The effect of physical and chemical aerosol properties on warm
731 cloud droplet activation, Atmos. Chem. Phys., 6, 2593–2649, doi:10.5194/acp-6-2593-2006,
732 2006.

733 Medina, J., Nenes, A., Sotiropoulou, R. E. P., Cottrell, L. D., Ziemba, L. D., Beckman, P. J., and
734 Griffin, R. J.: Cloud condensation nuclei closure during the International Consortium for
735 Atmospheric Research on Transport and Transformation 2004 campaign: Effects of size
736 resolved composition, J. Geophys. Res. Atmos., 112, D10S31, doi:10.1029/2006JD007588,
737 2007.

738 Mei, F., Setyan, A., Zhang, Q., and Wang, J.: CCN activity of organic aerosols observed
739 downwind of urban emissions during CARES, Atmos. Chem. Phys., 13, 12155–12169,
740 doi:10.5194/acp-13-12155-2013, 2013a.

741 Mei, F., Hayes, P. L., Ortega, A. M., Taylor, J. W., Allan, J. D., Gilman, J. B., Kuster, W. C., de
742 Gouw, J. A., Jimenez, J. L., and Wang, J.: Droplet activation properties of organic aerosols
743 observed at an urban site during CalNex-LA, J. Geophys. Res., 118, 2903-2917,
744 10.1002/jgrd.50285, 2013b.

745 Meng, J. W., Yeung, M. C., Li, Y. J., Lee, B. Y. L., and Chan, C. K.: Size-resolved cloud
746 condensation nuclei (CCN) activity and closure analysis at the HKUST Supersite in Hong Kong,
747 Atmos. Chem. Phys., 14, 10267–10282, doi:10.5194/acp-14-10267-2014, 2014.

748 Moore, R. H., Nenes, A., and Medina, J.: Scanning mobility CCN analysis—A method for fast
749 measurements of size-resolved CCN distributions and activation kinetics, Aerosol Sci. Technol.,
750 44, 861–871, doi:10.1080/02786826.2010.498715, 2010.

751 Moore, R. H., Cerully, K., Bahreini, R., Brock, C. A., Middlebrook, A. M., and Nenes, A.:
752 Hygroscopicity and composition of California CCN during summer 2010, J. Geophys. Res.
753 Atmos., 117, D00V12, doi:10.1029/2011JD017352, 2012.

754 Paatero, P., and U. Tapper (1994), Positive matrix factorization: A non-negative factormodel with
755 optimal utilization of error estimates of data values, Environmetrics, 5, 111–126.

756 Peng, J., Hu, M., Guo, S., Du, Z., Zheng, J., & Shang, D., et al. (2016). Markedly enhanced
757 absorption and direct radiative forcing of black carbon under polluted urban environments.
758 *Proceedings of the National Academy of Sciences of the United States of America, 113*(16),
759 4266.

760 Petters, M. D., and Kreidenweis, S. M.: A single parameter representation of hygroscopic growth

761 and cloud condensation nucleus activity, Atmos. Chem. Phys., 7, 1961–1971,
762 doi:10.5194/acp-7-1961-2007, 2007.

763 Riemer, N., Vogel, H., and Vogel, B.: Soot aging time scales in polluted regions during day and
764 night, Atmos. Chem. Phys., 4, 1885–1893, doi:10.5194/acp-4-1885-2004, 2004.

765 Rose, D., Gunthe, S. S., Mikhailov, E., Frank, G. P., Dusek, U., Andreae, M. O., and Pöschl, U.:
766 Calibration and measurement uncertainties of a continuous-flow cloud condensation nuclei
767 counter (DMT-CCNC): CCN activation of ammonium sulfate and sodium chloride aerosol
768 particles in theory and experiment, Atmos. Chem. Phys., 8, 1153–1179,
769 doi:10.5194/acp-8-1153-2008, 2008.

770 Rose, D., Nowak, A., Achtert, P., Wiedensohler, A., Hu, M., Shao, M., Zhang, Y., Andreae, M. O.,
771 and Pöschl, U.: Cloud condensation nuclei in polluted air and biomass burning smoke near the
772 mega-city Guangzhou, China. Part 1: Size-resolved measurements and implications for the
773 modeling of aerosol particle hygroscopicity and CCN activity, Atmos. Chem. Phys., 10,
774 3365–3383, doi:10.5194/acp-10-3365-2010, 2010.

775 Rosenfeld, D., Lohmann, U., Raga, G. B., O'Dowd, C. D., Kulmala, M., Fuzzi, S., Reissell, A.,
776 and Andreae, M. O.: Flood or drought: How do aerosols affect precipitation?, Science, 321,
777 doi:10.1126/science.1160606, 2008.

778 Sotiropoulou, R.-E. P., Medina, J., and Nenes, A.: CCN predictions: Is theory sufficient for
779 assessments of the indirect effect?, Geophys. Res. Lett., 33, doi:10.1029/2005gl025148, 2006.

780 Stokes, R. H., and Robinson, R. A.: Interactions in aqueous nonelectrolyte solutions. I.
781 Solute-solvent equilibria, J. Phys. Chem., 70, 2126–2130, 1966.

782 Sun, J., Zhang, Q., Canagaratna, M. R., Zhang, Y., Ng, N. L., Sun, Y., Jayne, J. T., Zhang, X.,
783 Zhang, X., and Worsnop, D. R.: Highly time- and size-resolved characterization of submicron
784 aerosol particles in Beijing using an Aerodyne Aerosol Mass Spectrometer, Atmos. Environ., 44,
785 131–140, doi:10.1016/j.atmosenv.2009.03.020, 2010.

786 Sun, Y. L., Wang, Z. F., Fu, P. Q., Yang, T., Jiang, Q., Dong, H. B., Li, J., and Jia, J. J.: Aerosol
787 composition, sources and processes during wintertime in Beijing, China, Atmos. Chem. Phys.,
788 13, 4577–4592, doi:10.5194/acp-13-4577-2013, 2013.

789 Sun, Y. L., Wang, Z. F., Du, W., Zhang, Q., Wang, Q. Q., Fu, P. Q., Pan, X. L., Li, J., Jayne, J., and
790 Worsnop, D. R.: Long-term real-time measurements of aerosol particle composition in Beijing,
791 China: Seasonal variations, meteorological effects, and source analysis, Atmos. Chem. Phys., 15,
792 10149–10165, doi:10.5194/acp-15-10149-2015, 2015.

Sun, Y., Chen, C., Zhang, Y., Xu, W., Zhou, L., Cheng, X., Zheng, H., Ji, D., Li, J., Tang, X., Fu, P., and Wang, Z.: Rapid formation and evolution of an extreme haze episode in Northern China during winter 2015, Sci. Rep., 6, doi:10.1038/srep27151, 2016.

Textor, C., Schulz, M., Guibert, S., Kinne, S., Balkanski, Y., Bauer, S., Berntsen, T., Berglen, T., Boucher, O., Chin, M., Dentener, F., Diehl, T., Easter, R., Feichter, H., Fillmore, D., Ghan, S., Ginoux, P., Gong, S., Grini, A., Hendricks, J., Horowitz, L., Huang, P., Isaksen, I., Iversen, I., Kloster, S., Koch, D., Kirkevåg, A., Kristjansson, J. E., Krol, M., Lauer, A., Lamarque, J. F., Liu, X., Montanaro, V., Myhre, G., Penner, J., Pitari, G., Reddy, S., Seland, Ø., Stier, P., Takemura, T., and Tie, X.: Analysis and quantification of the diversities of aerosol life cycles within AeroCom, Atmos. Chem. Phys., 6, 1777–1813, doi:10.5194/acp-6-1777-2006, 2006.

Twomey, S.: The influence of pollution on the shortwave albedo of clouds, J. Atmos. Sci., 34, 1149–1152, doi:10.1175/1520-0469(1977)034(1149: TIOPOT)2.0.CO;2, 1977.

Wang, J., Flagan, R. C., and Seinfeld, J. H.: A differential mobility analyzer (DMA) system for submicron aerosol measurements at ambient relative humidity, Aerosol Sci. Technol., 37, 46–52, 2003.

Wang, J., Cubison, M. J., Aiken, A. C., Jimenez, J. L., and Collins, D. R.: The importance of aerosol mixing state and size-resolved composition on CCN concentration and the variation of the importance with atmospheric aging of aerosols, Atmos. Chem. Phys., 10, 7267–7283, doi:10.5194/acp-10-7267-2010, 2010.

Wang, G., Zhang, R., Gomez, M. E., Yang, L., Zamora, M. L., Hu, M., ... & Li, J. (2016). Persistent sulfate formation from London Fog to Chinese haze. Proceedings of the National Academy of Sciences, 113(48), 13630-13635.

Wang, Y., Zhang, F., Li, Z., Tan, H., Xu, H., Ren, J., Zhao, J., Du, W., and Sun, Y.: Enhanced hydrophobicity and volatility of submicron aerosols under severe emission control conditions in Beijing, Atmos. Chem. Phys., 17, 5239–5251, doi:10.5194/acp-17-5239-2017, 2017.

Wiedensohler, A., Cheng, Y. F., Nowak, A., Wehner, B., Achtert, P., Berghof, M., Birmili, W., Wu, Z. J., Hu, M., Zhu, T., Takegawa, N., Kita, K., Kondo, Y., Lou, S. R., Hofzumahaus, A., Holland, F., Wahner, A., Gunthe, S. S., Rose, D., Su, H., and Pöschl, U.: Rapid aerosol particle growth and increase of cloud condensation nucleus activity by secondary aerosol formation and condensation: A case study for regional air pollution in northeastern China, J. Geophys. Res. Atmos., 114, D00G08, doi:10.1029/2008JD010884, 2009.

Wu, Y., Wang, X., Tao, J., Huang, R., Tian, P., Cao, J., Zhang, L., Ho, K.-F., Han, Z., and Zhang, R.: Size distribution and source of black carbon aerosol in urban Beijing during winter haze episodes, Atmos. Chem. Phys., 17, 7965–7975, doi:10.5194/acp-17-7965-2017, 2017.

827 Wu, Z. J., Zheng, J., Shang, D. J., Du, Z. F., Wu, Y. S., Zeng, L. M., Wiedensohler, A., and Hu, M.:
828 Particle hygroscopicity and its link to chemical composition in the urban atmosphere of Beijing,
829 China, during summertime, Atmos. Chem. Phys., 16, 1123–1138,
830 doi:10.5194/acp-16-1123-2016, 2016.

831 Yum, S. S., Hudson, J. G., Song, K. Y., and Choi, B. C.: Springtime cloud condensation nuclei
832 concentrations on the west coast of Korea, Geophys. Res. Lett., 32, L09814,
833 doi:10.1029/2005GL022641, 2005. :

834 Yum, S. S., Roberts, G., Kim, J. H., Song, K. Y., and Kim, D. Y.: Submicron aerosol size
835 distributions and cloud condensation nuclei concentrations measured at Gosan, Korea, during
836 the Atmospheric Brown Clouds East Asian Regional Experiment 2005, J. Geophys. Res. Atmos.,
837 112, D22S32, doi:10.1029/2006JD008212, 2007.

838 Zdanovskii, B.: Novyi Metod Rascheta Rastvorimostei Elektrolitovv Mnogokomponentnykh
839 Sistema, Zh. Fiz. Khim+, 22, 1478–1495, 1948.

840 Zhang, F., Li, Y., Li, Z., Sun, L., Li, R., Zhao, C., Wang, P., Sun, Y., Liu, X., Li, J., Li, P., Ren, G.,
841 and Fan, T.: Aerosol hygroscopicity and cloud condensation nuclei activity during the AC^3Exp
842 campaign: Implications for cloud condensation nuclei parameterization, Atmos. Chem. Phys.,
843 14, 13423–13437, doi:10.5194/acp-14-13423-2014, 2014.

844 Zhang, F., Li, Z., Li, Y., Sun, Y., Wang, Z., Li, P., Sun, L., Wang, P., Cribb, M., Zhao, C., Fan, T.,
845 Yang, X., and Wang, Q.: Impacts of organic aerosols and its oxidation level on CCN activity
846 from measurement at a suburban site in China, Atmos. Chem. Phys., 16, 5413–5425,
847 doi:10.5194/acp-16-5413-2016, 2016.

848 Zhang F., Wang Y., Peng J., Ren J., Zhang R., Sun Y., Don Collin., Yang X., Li Z.: Uncertainty
849 in predicting CCN activity of aged and primary aerosols. Journal of Geophysical
850 Research: Atmospheres. 10.1002/2017JD027058, 2017.

851 Zhang, Z., Engling, G., Lin, C.-Y., Chou, C. C. K., Lung, S.-C. C., Chang, S.-Y., Fan, S., Chan,
852 C.-Y., and Zhang, Y.-H.: Chemical speciation, transport and contribution of biomass burning
853 smoke to ambient aerosol in Guangzhou, a mega city of China, Atmos. Environ., 44, 3187–3195,
854 doi:10.1016/j.atmosenv.2010.05.024, 2010.

855 Zhao, J., Du, W., Zhang, Y., Wang, Q., Chen, C., Xu, W., Han, T., Wang, Y., Fu, P., Wang, Z., Li,
856 Z., and Sun, Y.: Insights into aerosol chemistry during the 2015 China Victory Day parade:
857 results from simultaneous measurements at ground level and 260 m in Beijing, Atmos. Chem.
858 Phys., 17, 3215–3232, doi:10.5194/acp-17-3215-2017, 2017.

859 Zheng, G. J., Duan, F. K., Su, H., Ma, Y. L., Cheng, Y., Zheng, B., Zhang, Q., Huang, T., Kimoto,

T., Chang, D., Pöschl, U., Cheng, Y. F., and He, K. B.: Exploring the severe winter haze in Beijing: the impact of synoptic weather, regional transport and heterogeneous reactions, Atmos. Chem. Phys., 15, 2969–2983, doi:10.5194/acp-15-2969-2015, 2015.

Zhang, Q., Worsnop, D. R., Canagaratna, M. R., and Jimenez, J. L.: Hydrocarbon-like and oxygenated organic aerosols in Pittsburgh: insights into sources and processes of organic aerosols, Atmos. Chem. Phys., 5, 3289–3311, doi:10.5194/acp-5-3289- 2005, 2005.

881 **Figures**

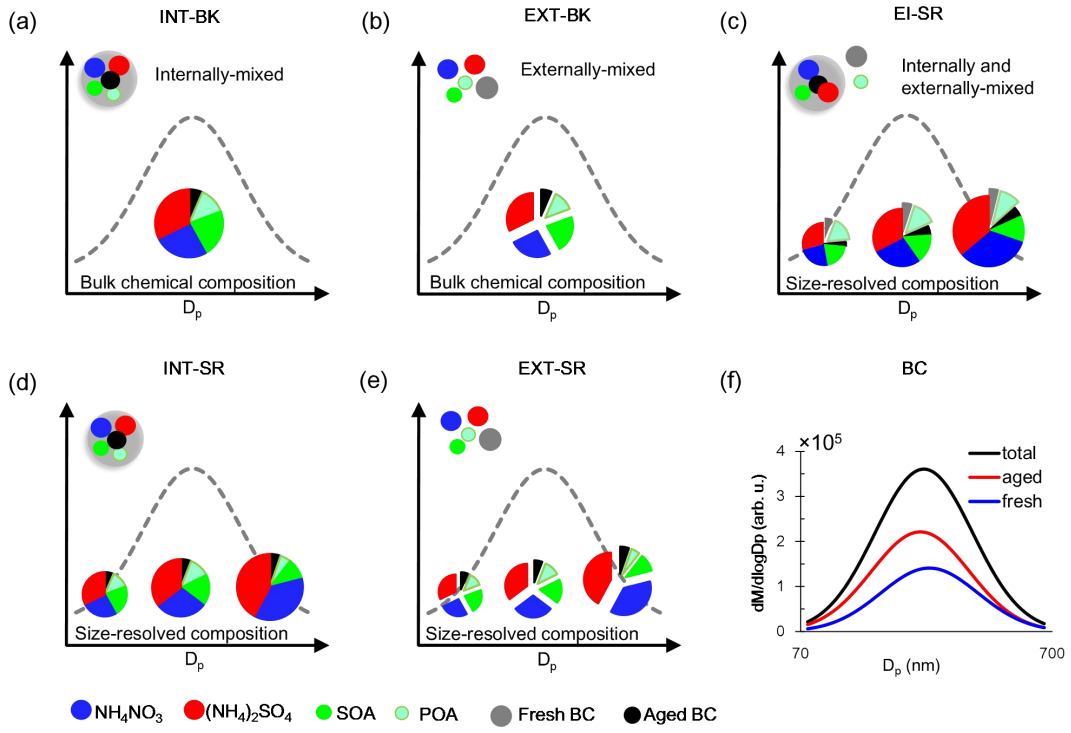

882

883 **Figure 1** Schematic representation of the five different schemes: (a) INT-BK, (b)

884 EXT-BK, (c) EI-SR, (d) INT-SR, and (e) EXT-SR. And the BC size distribution (f)

885 used in this study. The fresh and aged BC size distribution are retrieved from the total

886 BC size distribution measured by the SP2 (Wu et al., 2017) and the dependence of the

887 fraction of internally mixed soot (F_{in}) on particle diameter (D_p) observed in urban

888 Beijing (Cheng et al., 2012). The total BC size distribution is used in the INT-SR and

889 EXT-SR schemes, and the aged and fresh BC distributions are used in the EI-SR

890 scheme. In the EI-SR scheme, some BC particles are assumed to already be aged and

891 thus internally-mixed with sulfate, nitrate and SOA, and some of them together with

892 POA are freshly emitted and assumed not yet aged/coated by other species

893 (externally-mixed).

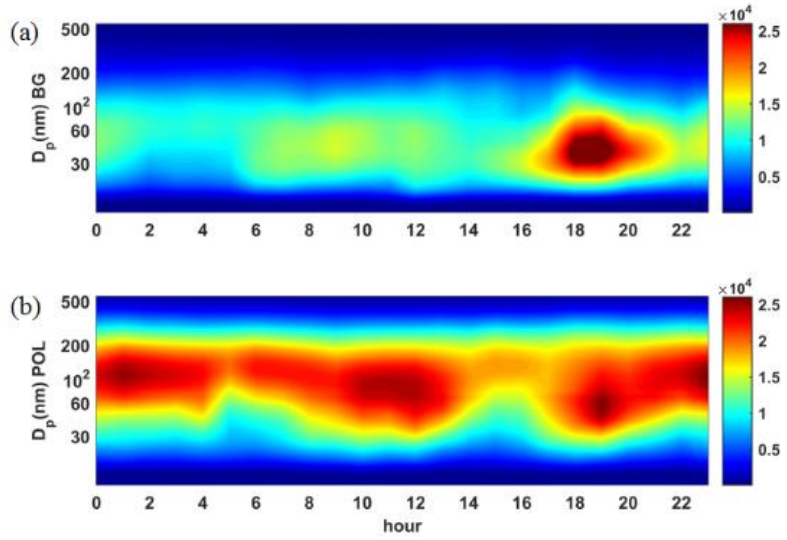

894

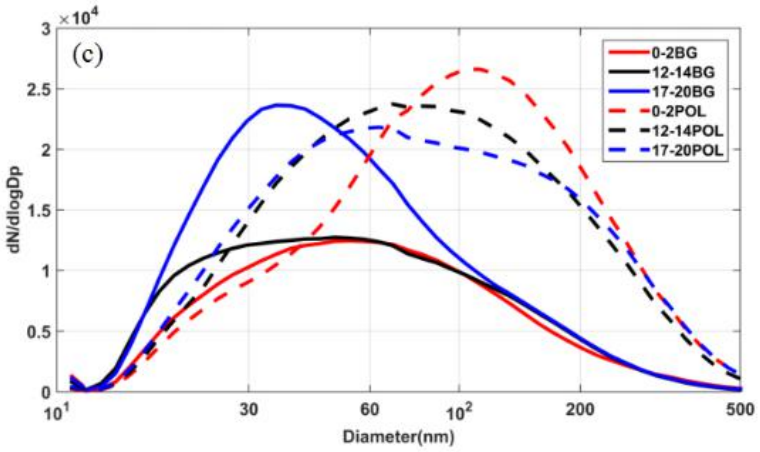

895

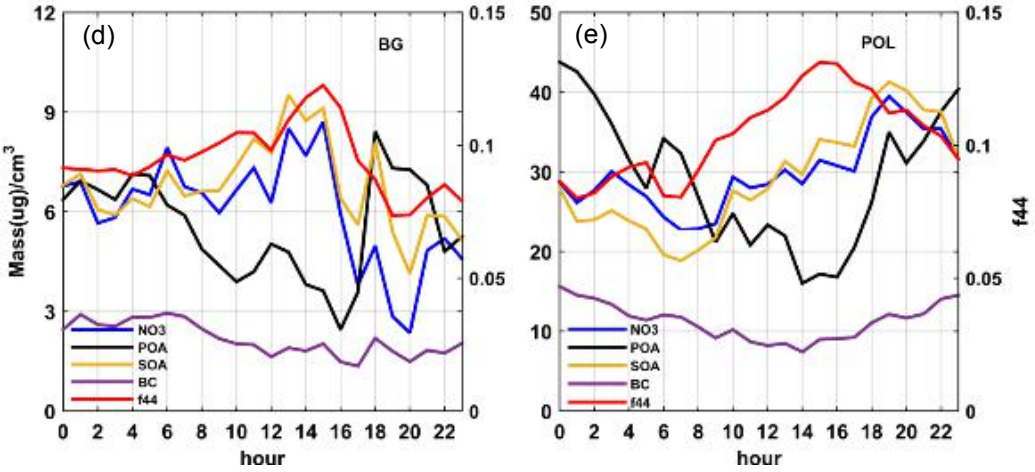

896

897 **Figure 2.** Diurnal variations in aerosol properties at the IAP site during the APHH

898 field experiment, including the particle number size distribution measured by the

SMPS under (a) background (BG) and (b) polluted (POL) conditions; (c) mean particle number size distribution measured by the SMPS during three periods (0000–0200 LT, 1200–1400 LT, and 1700–2000 LT) under BG and POL conditions; bulk chemical component mass concentrations (NO_3, POA, SOA, and BC) and f_{44} made under (d) BG and (e) POL conditions.

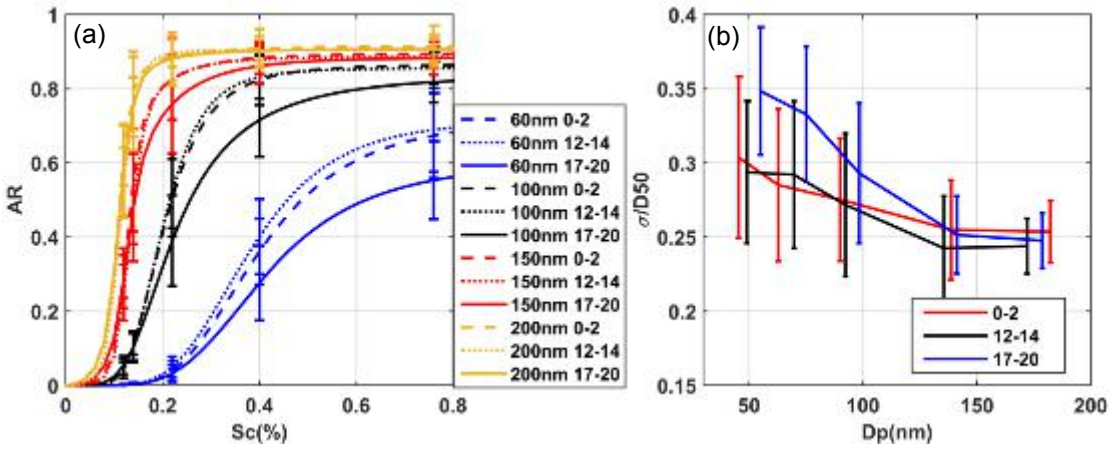

905

906 **Figure 3.** (a) Averaged fitted CCN efficiency spectra during the nighttime period

907 (0000–0200 LT, dashed lines), the noontime period (1200–1400 LT, dotted lines) and

908 the evening rush hour period (1700–2000 LT, solid lines) for different diameters (60,

909 100, 150, and 200 nm); (b) the heterogeneity of aerosol particles (σ_a/D_a) derived from

910 Equation (7) during the three selected periods.

911

912

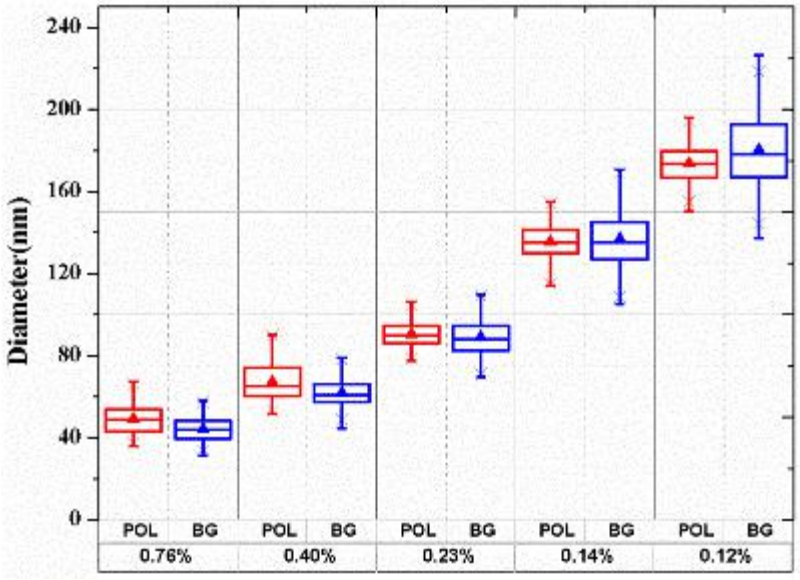

913

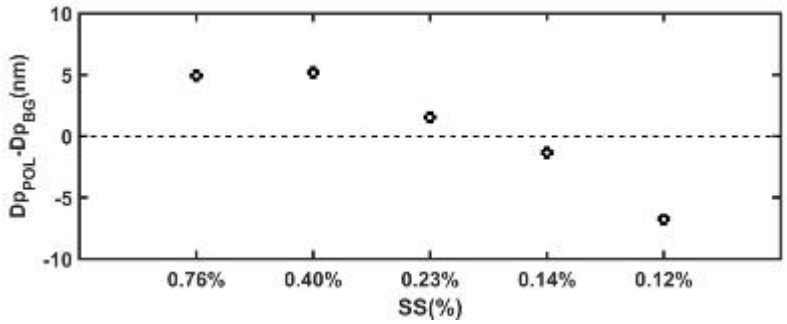

914 **Figure 4.** Top: Retrieved mean critical activation diameters at SS = 0.12, 0.14, 0.23,
915 0.40, and 0.76% under background (BG) and polluted (POL) conditions. The box
916 plots show mean critical activation diameters at the 25th, 50th, and 75th percentiles.
917 Bottom: Difference in the mean critical activation diameter between BG and POL
918 cases.

919

920

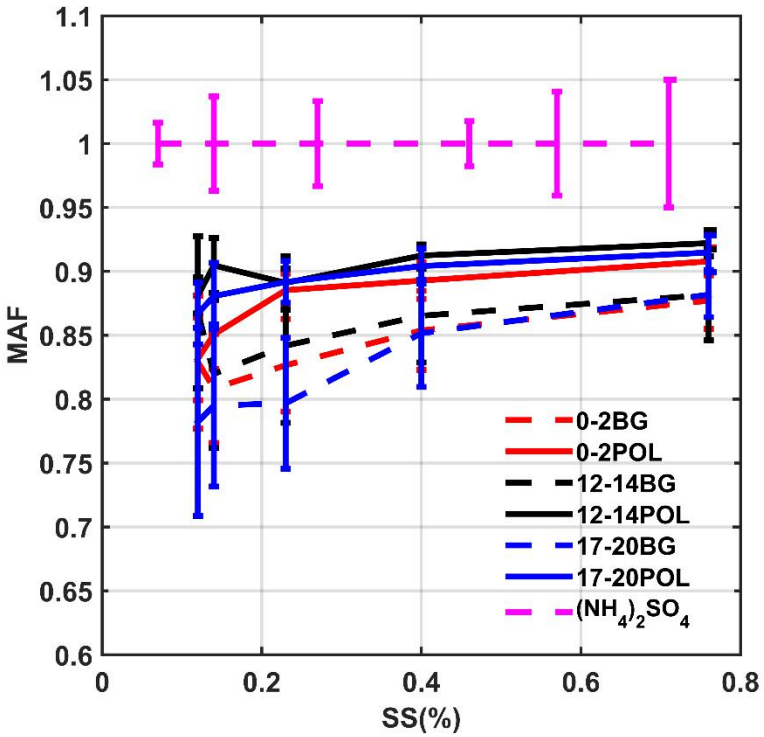

921

922 **Figure 5.** Mean maximum active fractions (MAFs) of CCN activation spectra under

923 polluted (POL) and background (BG) conditions during the three periods, i.e.,

924 0000–0200 LT, 1200–1400 LT, and 1700–2000 LT. The MAF of pure $(NH_4)_2SO_4$

925 particles at the different SS levels (magenta line) is also plotted.

926

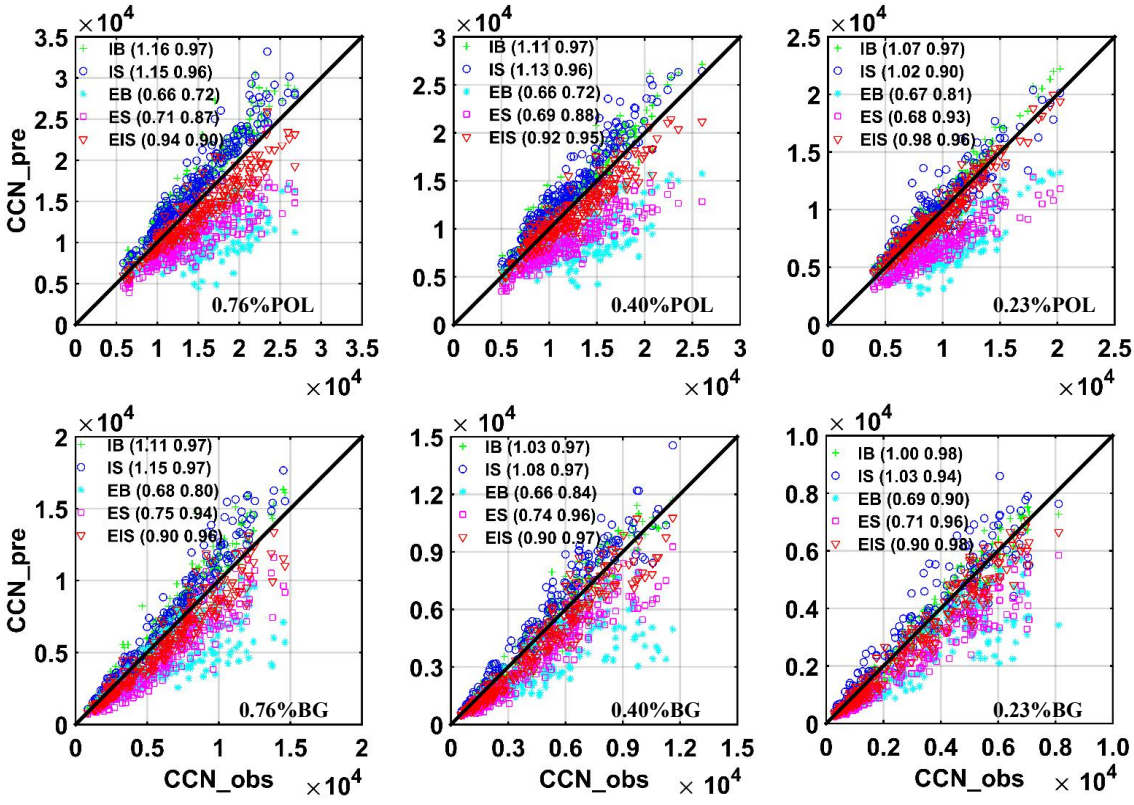

+ **INT-BK Internal mixture, bulk composition**

o **INT-SR Internal mixture, size-resolved composition**

* **EXT-BK External mixture, bulk composition**

□ **EXT-SR External mixture, size-resolved composition**

▽ **EI-SR External mixture, POA and BC externally mixed, size-resolved composition**

Figure 6. Predicted N_{CCN} as a function of measured N_{CCN} using the five assumptions (colored symbols) at three supersaturation levels (0.23, 0.40, and 0.76%) under polluted (POL) and background (BG) conditions. The numbers in parentheses are the slope (first number) and the correlation coefficient (second number).

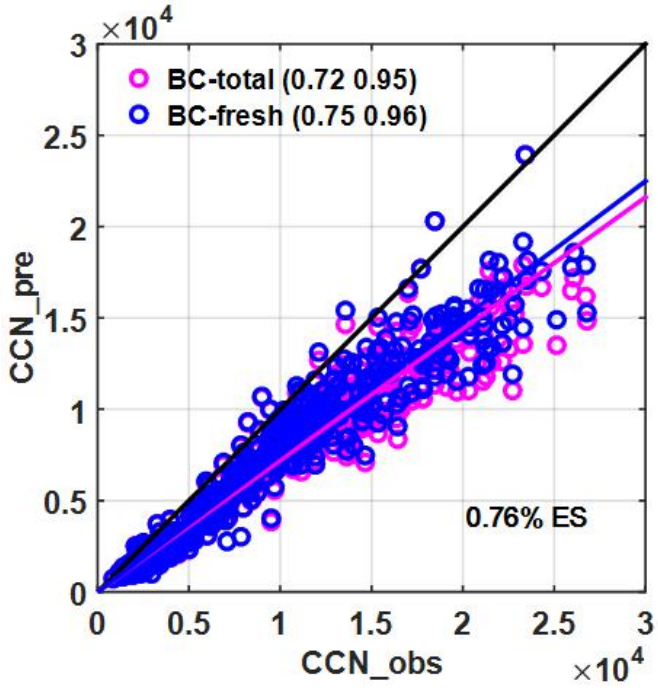

Figure 7. Predicted N_{CCN} as a function of measured N_{CCN} using the EXT-SR assumption (colored symbols) at S=0.76%. The pink and blue circles denote the results predicted by using total and fresh BC size distributions, respectively. The numbers in parentheses are the slope (first number) and the correlation coefficient (second number).

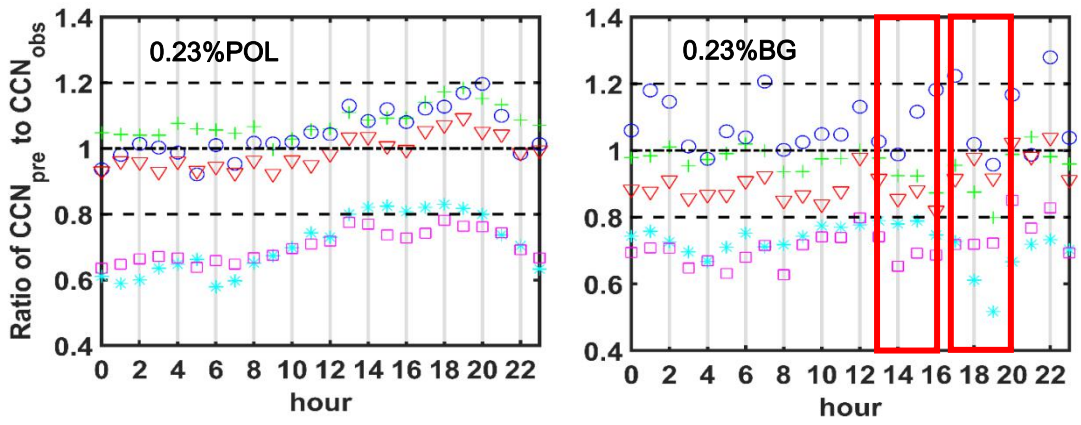

+ **INT-BK Internal mixture, bulk composition**

o **INT-SR Internal mixture, size-resolved composition**

* **EXT-BK External mixture, bulk composition**

□ **EXT-SR External mixture, size-resolved composition**

▽ **EI-SR External mixture, POA and BC externally mixed, size-resolved composition**

Figure 8. Diurnal variations in the ratio of predicted-to-measured N_{CCN} at a supersaturation level of 0.23% under background (BG) and polluted (POL) conditions.

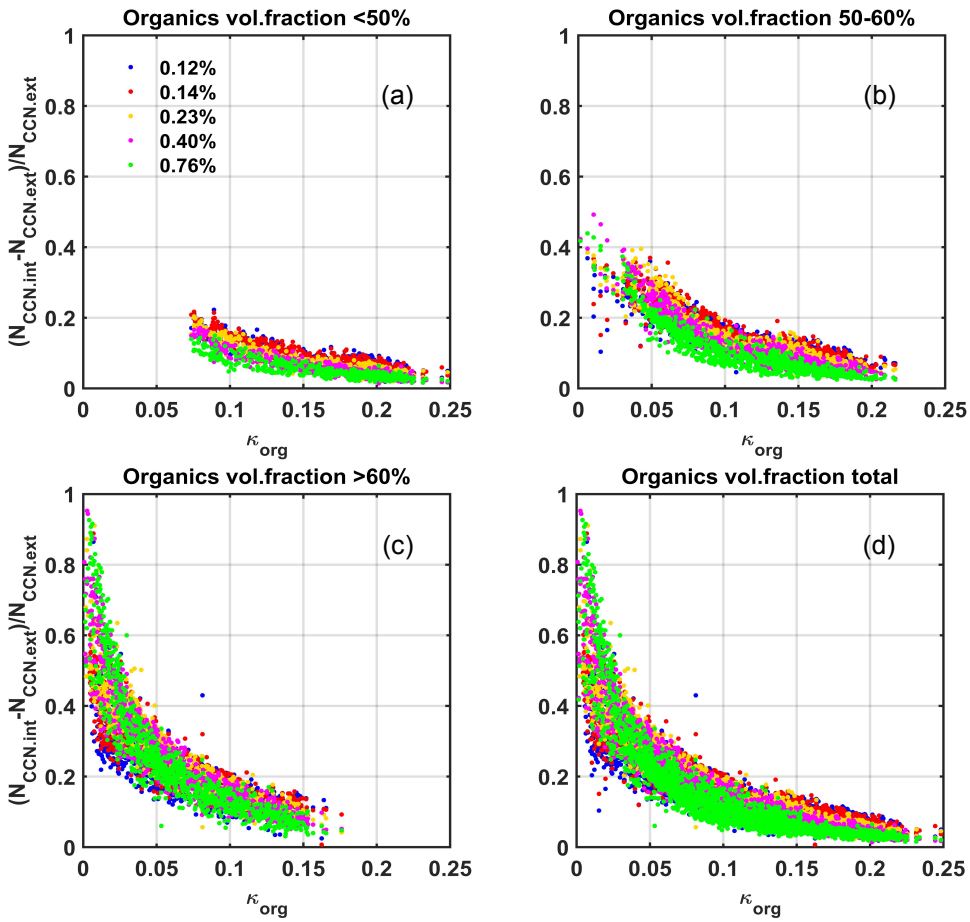

Figure 9. Relative deviations between N_{CCN} predicted under the assumptions of internal (INT-BK) and external (EXT-BK) mixtures [(N_{CCN}.INT-BK - N_{CCN}.EXT-BK) (N_{CCN}.EXT-BK)$^{-1}$] as a function of κ_{org} when organic volume fractions of <50 (a), 50-60 (b), >60% (c) and all observed data points (d). The solid with different colors represent different supersaturation levels. The different colors denote the different organic fractions.